Spectral features and antibacterial properties of Cu-doped ZnO nanoparticles prepared by sol-gel method*

Alireza Samavati[1,2], A F Ismail[2,†], Hadi Nur[1], Z Othaman[1], and M K Mustafa[3]

[1] *Centre for Sustainable Nanomaterials, Ibnu Sina Institute for Scientific and Industrial Research, Universiti Teknologi Malaysia,* 81310 *UTM, Skudai, Johor, Malaysia*

[2] *Advanced Membrane Technology Research Centre (AMTEC), Universiti Teknologi Malaysia,* 81310, *Skudai, Johor, Malaysia*

[3] *Faculty of Science Technology and Human Development, Universiti Tun Hussein Onn Malaysia,* 86400 *Parit Raja, Johor, Malaysia*

(Received 31 January 2016; revised manuscript received 21 March 2016; published online 1 June 2016)

$Zn_{1-x}Cu_xO$ ($x = 0.00$, 0.01, 0.03, and 0.05) nanoparticles are synthesized via the sol-gel technique using gelatin and nitrate precursors. The impact of copper concentration on the structural, optical, and antibacterial properties of these nanoparticles is demonstrated. Powder x-ray diffraction investigations have illustrated the organized Cu doping into ZnO nanoparticles up to Cu concentration of 5% ($x = 0.05$). However, the peak corresponding to CuO for $x = 0.01$ is not distinguishable. The images of field emission scanning electron microscopy demonstrate the existence of a nearly spherical shape with a size in the range of 30–52 nm. Doping Cu creates the Cu–O–Zn on the surface and results in a decrease in the crystallite size. Photoluminescence and absorption spectra display that doping Cu causes an increment in the energy band gap. The antibacterial activities of the nanoparticles are examined against Escherichia coli (Gram negative bacteria) cultures using optical density at 600 nm and a comparison of the size of inhibition zone diameter. It is found that both pure and doped ZnO nanoparticles indicate appropriate antibacterial activity which rises with Cu doping.

Keywords: Cu-doped ZnO nanoparticles, photoluminescence, antibacterial, E. coli

PACS: 78.67.Bf, 78.55.–m, 87.55.de **DOI:** 10.1088/1674-1056/25/7/077803

1. Introduction

ZnO has been the most commonly and extensively studied material in the field of nano science and technology. It is because of the unique characteristics of this material, such as extensive band gap energy (3.37 eV), electrical and thermal stability, large exciton binding energy (60 meV), and large saturation velocity (3.2×10^7 cm·s^{-1}).[1] Due to these tremendous properties, ZnO nanoparticles have been extensively used in light-emitting diodes, laser diodes, solar cells, microelectronic, surface acoustic wave devices, hydrogen-storage devices, transparent electrodes, transparent thin-film transistors, antibacterial coating, UV protectors, targeted drug delivery and sensors.[2–5] ZnO is an inorganic antibacterial agent and has enormous advantages due to biocompatibility, action against bacteria in the neutral region (pH 7) even in darkness, non-toxicity to humans, ability to withstand harsh conditions, and being more durable compared to the conventional organic materials.[6] Therefore, these unique properties make it the right candidate for antibacterial applications and suitable for industrial usage. For controlling the growth of ZnO nanostructures, several synthesis methods are developed including sol–gel, hydrothermal, solvothermal, sonochemical, combustion, magnetron sputtering, and pulsed laser deposition.[7–12] The crystallite size effects play a predominant role on the properties of ZnO particles especially in nanometric dimensions where defects become significant. Furthermore, doping of different elements is considered as a promising route to tune the properties of ZnO nanoparticles.[13–16] The different ionic radii of the dopants and zinc greatly affect the crystallite size and lattice parameters. Consequently, it is necessary to include these effects in the crystallite calculations. Crystallite size and lattice strain are the two main factors that lead to widening of the diffraction peaks. Lattice strain is originated from the lattice imperfection or dopants which in turn alter the peak intensity and position.[17] Moreover, the uniform and non-uniform strain change the peak position and increase the peak broadening respectively.

Recently, using metal oxides antibacterial coatings in order to prevent the infections in particular non-selective microbicides such as reactive oxygen species (ROS) has improved.[18] Although, antibacterial activity of pure ZnO has been studied in different morphologies using mechanisms such as generation of ROS, hydroxyl radicals, hydrogen peroxide, superoxide anions O^{2-}, the release of Zn^{2+} ions, cell membrane damage, the accumulation of nanoparticles in cytoplasm and outer membranes, many scientists believe that these nanoparticles are known to be toxic for humans.[19–23] Our results illustrate that at a relatively low concentration of dopant, a respectable action against the bacterial pathogens takes place; this hypothesis is in agreement with many other reports.[24,25] Despite many efforts, the antibacterial potency of Cu-doped ZnO nanoparticles against bacterium is still far

*Project supported by the Universiti Teknologi Malaysia (UTM) (Grant No. R. J1300000.7809.4F626). Dr. Samavati is thankful to RMC for postdoctoral grants.

†Corresponding author. E-mail: afauzi@utm.my

© 2016 Chinese Physical Society and IOP Publishing Ltd

from being understood. Accurate synthesis methods and systematic characterizations are pre-requisite for such understanding. This study is an attempt to enhance and optimize the antibacterial behavior of ZnO nanoparticles through Cu doping. For this aim, nanoparticles of ZnO doped with Cu are synthesized via the sol-gel method and the effects of dopants concentration on the structural and optical behavior as well as antibacterial activity are investigated.

2. Experimental

For synthesizing the ZnO nanoparticles, raw materials of zinc nitrate hexahydrate (Zn $(NO_3)_2.6H_2O$), copper nitrate hexahydrate (Cu $(NO_3)_2.6H_2O$), gelatin ($(NHCOCH–R_1)_n$, R_1 = amino acid, Type A, Porsin), and distilled water are employed. A batch of 2g of the final product is acquired by dissolving the particular amount of copper and zinc nitrates into 20 ml of distilled water. The nitrates amount are measured according to the $Zn_{1-x}Cu_xO$ formula, where $x = 0.00$, 0.01, 0.03, and 0.05. Approximately 4 g of gelatin with the final ratio of 2:1 are slowly added to 60 ml of distilled water and then the solution is stirred at 80 °C in an oil bath. A clear solution is achieved after completely dissolving the gelatin in water. Then, Zn^{2+} and Cu^{2+} solutions are added to the gelatin solution. The temperature is kept constant at 80 °C for 6 hours. The mixture is continuously stirred to obtain a clear, viscose, and honey-like gel. In order to calcine, a small volume of the prepared gel was scrubbed on the alumina crucible's inner walls before putting it into the furnace. The furnace temperature is kept at 600 °C for 2 hours with a heating speed of 5 °C/min.

The antibacterial activity of the prepared nanoparticles in the form of nanofluids is examined by calculating the growth curve of E. coli HB 101 protected in the LB broth medium.[26] The growth curves are obtained by determining the time growth of optical density (OD) for pure and Cu doped samples. The measurements are performed at 600 nm wavelength using a UV/Vis spectrophotometer (WPA LightWave S2000) at a frequency of once in an hour. For further analysis of the antibacterial properties of the samples, the following procedures is carried out. Briefly, the colloidal suspensions of the synthesized nanoparticles (2 mg/ml) are applied to agar plates in which E. coli bacterium is cultured. After 24 hours of incubation of the agar plates, the inhibition zone diameter is measured in millimeters (mm).

The structural properties of samples are investigated using Cu-$K\alpha$ radiation (0.154 nm) at 40 kV and 100 mA for x-ray diffraction (XRD) equipment built by a D8 Advance Diffractometer, Bruker, USA. The 2θ range is set to 20°–80° with a resolution and step size of 0.011° and 0.02°, respectively. The field-emission scanning electron microscopes (FESEM, JEOLJSM 6380LA) attached with EDX are employed for observing nanoparticles, size calculation, and elemental analysis. Fourier transformed infrared (FTIR) spectra are recorded using a Perkin Elmer 5DX FTIR. Room temperature photoluminescence (PL) spectra are recorded by employing a luminescence spectrometer (LS 55, Perkin Elmer, USA) under 239 nm excitation wavelength.

3. Results and discussion

The powder x-ray diffraction patterns are used to study the structural properties and the phase purity of the samples. Figure 1(a) illustrates the XRD patterns of the synthesized pure and Cu-doped ZnO nanoparticles and figure 1(b) shows the variation in intensity and position of the (101) peak. The detected peaks are certainly indexed as ZnO hexagonal wurtzite structure verified by PDF Code: 00-036-1451.

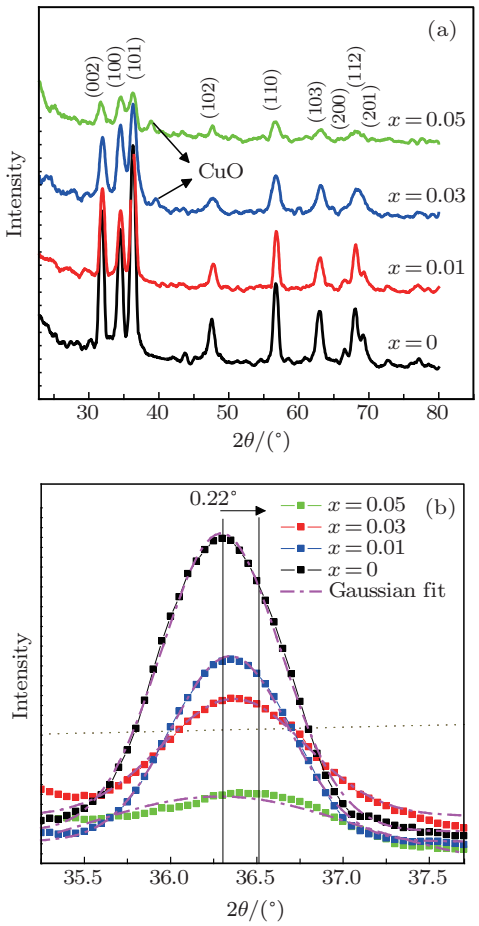


Fig. 1. (color online) (a) XRD patterns of Cu-doped ZnO nanoparticles having different dopant concentration. The small peak related to CuO (111) is shown by arrows. (b) Shift and broadening in the (101) diffraction peak due to changing Cu concentration.

The enhancement of Cu contents causes a decrease in the intensity of all diffraction peaks. This diminution is ascribed to the impacts of defects or disorders created by the copper ions in the ZnO lattice structure. In addition, no signal of Cu related phase such as metallic copper, oxides of copper, or any

binary zinc copper phase is identified for $x = 0.01$ sample, or the CuO peaks for the Cu-doped at $x = 0.01$ are too small to distinguish. This specifies that the Cu ions have substituted Zn sites without considerably altering the crystal structure of ZnO, which is associated to the fact that the ionic radius of Cu^{+2} (0.73 Å) is very close to that of Zn^{+2} (0.74 Å). Therefore, Cu can simply penetrate into ZnO crystal lattice. However, by increasing the doping percentage of Cu ($x = 0.03$), a very weak signal corresponding to CuO appears, and its intensity increases with further increase in Cu doping ($x = 0.05$). Therefore, it can be concluded that the segregating of CuO is started from $x = 0.03$ Cu concentration. It can be understood that for a smaller amount of Cu, its ions substitute well with Zn ions, but increasing Cu concentration causes a CuO cluster to form and isolate as an impurity phase.

The wurtzite lattice parameters such as the values of d, the distance between adjacent planes in the Miller indices (hkl) (calculated from the Bragg equation, $n\lambda = 2d\sin\theta$), lattice constants (a and c), and unit cell volumes are calculated from the lattice geometry equation[27]

$$\frac{1}{d^2} = \frac{4}{3}\left(\frac{h^2+hk+k^2}{a^2}\right) + \frac{l^2}{c^2}. \quad (1)$$

The lattice parameters of the samples are recorded in Table 1.

Table 1. Cu concentration dependent nanoparticles XRD peak positions, lattice parameters, and volume.

Compounds	$2\theta \pm 0.01$	hkl	$d_{hkl} \pm 0.0005$/nm	Lattice parameter	$V \pm 0.0002$/Å^3
Zn	36.29	(101)	0.2472	$a = 0.3252$	0.0477
($x = 0.00$)	34.39	(002)	0.2604	$c = 0.5208$	
$Zn_{0.99}Cu_{0.01}$	36.36	(101)	0.2467	$a = 0.3250$	0.0476
($x = 0.01$)	34.43	(002)	0.2601	$c = 0.5204$	
$Zn_{0.97}Cu_{0.03}$	36.43	(101)	0.2463	$a = 0.3247$	0.0474
($x = 0.03$)	34.47	(002)	0.2598	$c = 0.5198$	
$Zn_{0.95}Cu_{0.05}$	36.51	(101)	0.2458	$a = 0.3245$	0.0473
($x = 0.05$)	34.55	(002)	0.2592	$c = 0.5196$	

Cu doping results in a decrease in the lattice parameters 'a' and 'c', as compared to un-doped ZnO. This is attributed to a little mismatch in ionic radius between Zn^{+2} and Cu^{+2}. However, a systematic variation in lattice parameters with increasing Cu content does not exist. The c/a parameter is close to the value of 1.633, which indicates the existence of a close packed hexagonal structure.

The size of nanoparticles calculated using the x-ray line broadening method via the Scherrer equation ($D = k\lambda/\beta\cos\theta$), where k is a constant equal to 0.94, D and λ are the particle size in nanometers and wavelength of the radiation (1.54056 Å for Cu Kα radiation), respectively. β and θ are the peak width at half-maximum intensity and peak position, respectively. The instrument and sample both affect the Bragg peak FWHM and the broadening in the XRD peaks is a combination of them. For decoupling these contributions and determining the instrumental broadening, a diffraction pattern from the line broadening of a standard material such as silicon needs to be assembled. The instrument modified broadening (β_D) corresponding to the diffraction peak of ZnO nanoparticles with a Gaussian profile is estimated using the following equation:

$$\beta_{\rm D}^2 = \beta_{\rm measures}^2 - \beta_{\rm instrumental}^2.$$

Therefore, the Scherrer equation is modified as follows:

$$\cos\theta = \frac{\lambda k}{D}\left(\frac{1}{\beta_{\rm D}}\right). \quad (2)$$

Plots are drawn with $1/\beta_{\rm D}$ on the x axis and $\cos\theta$ along the y axis for the pure and Cu-doped ZnO nanoparticles prepared at different dopant concentrations.[27] By fitting the data, the crystallite size D is calculated from the slope of the fit line which is demonstrated in Fig. 2. The estimated crystallite size is obtained to be ~ 52, ~ 46, ~ 37, and ~ 30 nm by Scherer plot for $x = 0.00$, 0.01, 0.03, and 0.05 samples, respectively.

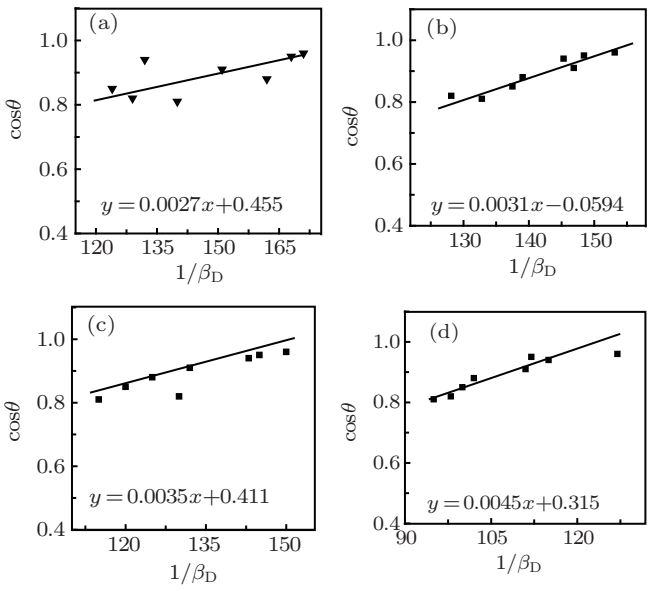


Fig. 2. Plot of $\cos\theta$ against $1/\beta_{\rm D}$ (Scherrer) for all prepared samples. (a) $x = 0$, (b) $x = 0.01$, (c) $x = 0.03$, and (d) $x = 0.05$.

The morphology and chemical composition of the synthesized nanoparticles are examined via FESEM coupled with EDX. The top view FESEM images of pure and Cu-doped

ZnO with various concentrations of Cu ($x = 0.01$, 0.03, and 0.05) as well as EDX mapping for the $x = 0.03$ sample are presented in Fig. 3. The inset shows a high magnification of the selected area. FESEM and EDX mapping images reveal the formation of homogeneous and uniform distributed nanoparticles. Cu doping strongly influences the grain size and morphology of ZnO nanoparticles. The average particle size is found to decrease with the increase in Cu doping into the ZnO matrix. The decrease in the particle size is mostly ascribed to the formation of Cu–O–Zn on the surface of the doped nanoparticles, which prevents the growth of crystal grains and assists separation of particles.

The presence of Cu and its homogenous distribution into ZnO nanoparticles is confirmed with the help of the EDX technique. Furthermore, the EDX spectra indicate that the nanoparticles are composed of Zn, O, Cu, Au, and C. A weak peak for C and Au is attributed to the supporter carbon tape and Au thin coating for FESEM image purpose.

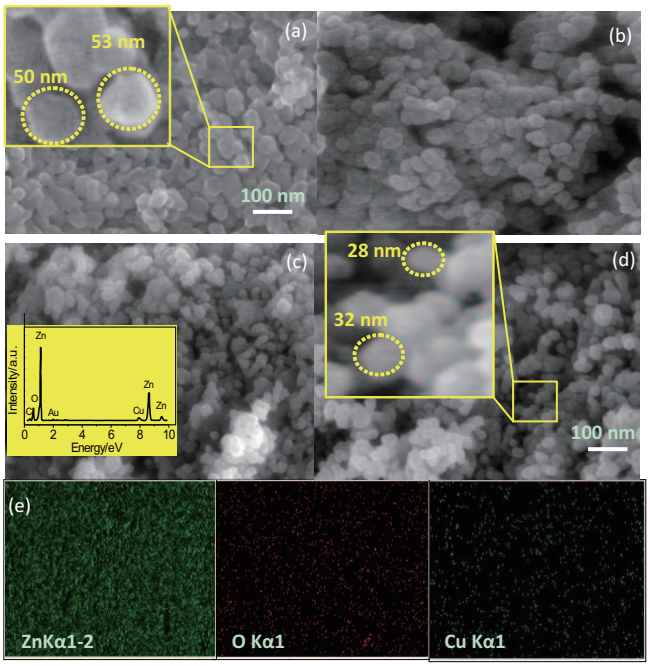


Fig. 3. (color online) Top-view FESEM images of samples. Insets (a) and (d) show the high magnification of the selected area and inset (c) is the EDX spectra for $Zn_{0.97}Cu_{0.03}O$ sample. EDX mapping images of Zn, O, and Cu for $Zn_{0.97}Cu_{0.03}O$ sample (e).

Figure 4 demonstrates the FTIR spectra of pure and Cu-doped ($x = 0.05$) ZnO nanoparticles. The inset shows the same plot in the range from 400 to 900 cm^{-1}. The high intensity absorption peaks from the vibration of hydroxyl group at ~ 3450 cm^{-1} and ~ 1600 cm^{-1} are attributed to the O–H stretching vibrations, which are related to the absorbed water on the surface of the samples. The origin of absorption at ~ 2380 cm^{-1} is the presence of CO_2 molecules in the environment.[28] Figure 4 indicates that for the un-doped sample, the intense absorption peak at ~ 435 cm^{-1} is related to the stretching vibrations of the Zn–O bond. In the doped sample, an absorption band near 620 cm^{-1} is also distinguishable, which is related to the vibration of the Cu–O bond.[29] Furthermore, the intensity of peak related to the Cu–O bond for the $x = 0.03$ sample is decreased and for $x = 0.01$ one is not distinguishable. Thus, both are not shown here.

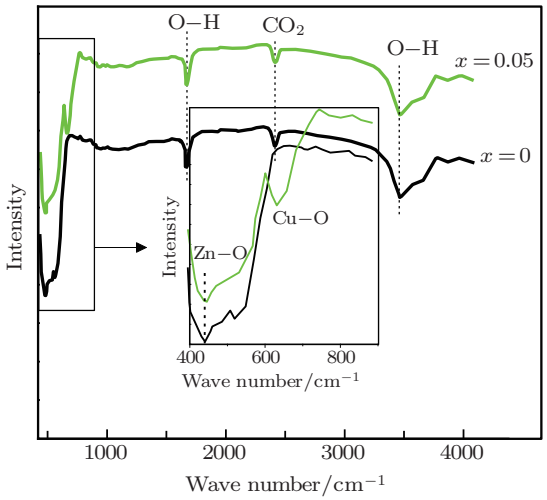


Fig. 4. (color online) FTIR spectra of pure and doped ($x = 0.05$) ZnO nanoparticles. Inset: the same FTIR spectra in the range of 400–900 cm^{-1}.

Figure 5 illustrates the room temperature PL spectra of the samples. For un-doped ZnO nanoparticles a strong peak at ~ 3.25 eV accompanied with a weak green signal associated with a deep-level emission in the visible region (~ 1.85 eV) are clearly seen. By increasing the Cu concentration a blue shift of ~ 0.13 eV occurs. Furthermore, enhancing the Cu concentration causes increment of the UV intensity near bandgap luminescence and the green emission (visible luminescence) related to deep centers. This demonstrates that the Cu-doped ZnO nanoparticles possess more enhanced optical features than un-doped nanoparticles. The formation of a smaller amount of non-radiative recombination channels in the sample with the higher Cu concentration may be attributed to the different origin of this peak. The visible luminescence which is located at ~ 1.85 eV could be ascribed to a deep unidentified acceptor with the energy level situated close to the middle of the bandgap.[30]

The near-bandgap PL spectrum of all samples shows a broad band which is related to the superposition of the band originated from recombination of free excitons with its longitudinal optical (LO) phonon. In addition, the PL spectra of sample $x = 0.05$ exhibit a broad band with the maximum at ~ 2.4–2.5 eV energy (see Fig. 5). This band is probably associated with the Cu impurity.[31,32] Typically, in this spectral range for Cu-doped ZnO nanoparticles, two noticeable types of bands connected with Cu impurity. The first one is a structured luminescence band, which is assigned to the internal transition of a hole in the Cu_{Zn} center from the excited state

approximately at 0.4 eV above the valence band and 0.2 eV below the conduction band.[33] The fine structure of the emission spectrum is due to multiple phonon replicas, which is associated with LO and local or pseudo-local vibration modes. The next is the structure-less green luminescence band which is ascribed to transitions from a shallow donor to the Cu^{+} state of a neutral Cu_{Zn} acceptor with a level nearly 0.5 eV beyond the maximum of the valence band.[34] The PL band detected in our samples is structure-less. The formation of complex defects $[Cu_{Zn}\text{-}Zn_i]^x$ in Cu–ZnO is probable by considering the broad PL bands in deep-level emission regions.

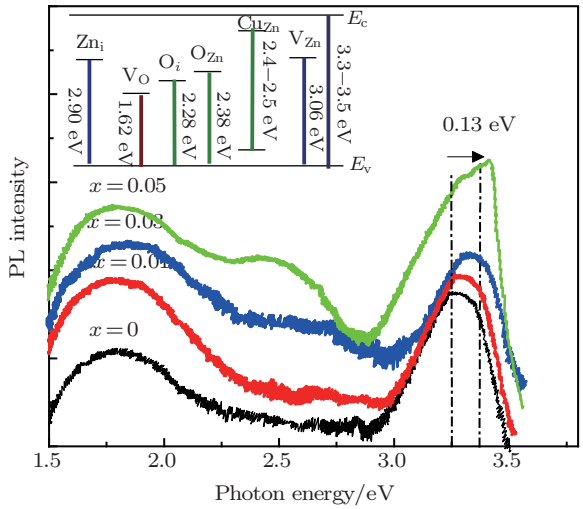


Fig. 5. (color online) Room temperature PL spectra of Cu-doped ZnO nanoparticles at different concentrations. Inset shows the band structures and possible electron and hole recombination.

UV–vis photons are passed through the pure and Cu-doped ZnO nanoparticles for further understanding of optical properties. Figure 6 indicates the recorded absorption spectra of samples. ZnO has four oxygen atoms which are coordinated to the tetrahedral Zn atoms. Zn d electrons hybridize with the oxygen p electrons to form an energy band gap and lead to the occurrence of absorption. For the ZnO structure, the absorption value normally appeared at around 400 nm.[35] The absorbance value in the visible region increases with increasing cu dopant. Moreover, the absorption edge is changed owing to incorporation of Cu ions into the ZnO crystallographic planes. The band gap energy value of pure and Cu-doped ZnO nanoparticles is calculated using Tauc's method, where extra plotting the linear portion of the curve to zero absorption edge gives the optical band gap of material, as depicted by Fig. 6. The band gap values are found to be ~ 3.25, ~ 3.28, ~ 3.31, and ~ 3.35 eV for $x = 0.00$, 0.01, 0.03, and 0.05 respectively. Without changing the ZnO crystal structure, the Cu ions hybridize with host electronic states that allow the variation of the energy bandgap. The increase in the energy bandgap value for Cu-doped ZnO nanoparticles is ascribed to the competitive effect of Burstein–Moss[36] and the degree of crystallization.[37] The Fermi level in nominally doped semiconductors located between valence and conduction bands. Through increasing the doping concentration, electrons' population situation remains within the conduction band. It pushes the Fermi level to higher energy and in the case of the degeneration level of the dopant, it stays inside the conduction band. Therefore, for degenerate semiconductors, the electron excitation only occurs from the top of the valence band into the conduction band above the Fermi level, which at this instant stays within conduction band. It should be noted that all the states below the Fermi level are occupied. Excitation into these occupied states is forbidden according to Pauli's exclusion principle. Therefore, Burstein–Moss results in a shift toward lower energy. On the other hand, the existence of disorders, lower degree of crystallinity, and probably the formation of a new compound by increasing the Cu content causes a shift to a higher energy. Consequently, the competition of these two phenomena leads to the enhancement in the apparent band gap.

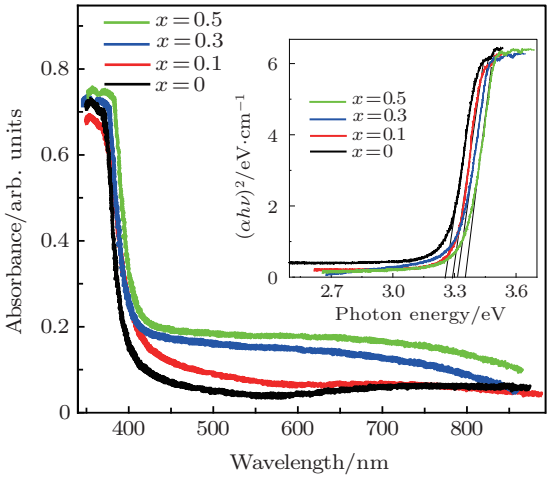


Fig. 6. (color online) Cu concentration dependent UV–visible absorption spectra of ZnO nanoparticles. Inset shows the bandgap value for samples calculated using Tauc's method.

Through developing the microorganism's resistance against the majority of antibiotics, the advanced research for finding a novel antibiotic becomes inevitable. Therefore, the present work is carried out to find the effect and properties of Cu-doped ZnO nanoparticles having different Cu concentration on killing curves of bacterial pathogens. The growth curve of E. coli bacteria in the presence of pure and Cu-doped ZnO nanoparticles with different dopant concentrations are illustrated in Fig. 7 (the inset shows the same optical density plot in the range of 0–0.5 for clear comparison). The negative control growth curve which is the plot of optical density for pure bacterial culture without the addition of nanoparticles is shown for comparison. The value of optical density at 600 nm represents the absorbance of the bacteria. Thus, the increasing number of bacteria indicates more light being absorbed by them. It is clearly seen that Cu doping improves

the antibacterial activity and also increasing Cu concentration causes enhancement of this antibacterial property. According to the McFarland standard the absorption of 0.2 for E. coli bacteria is approximately equivalent to a bacterial cell population of 3×10^8. Therefore, it can be seen from the inset of Fig. 7 that increasing Cu concentration has a significant effect on the killing of bacterial pathogens.

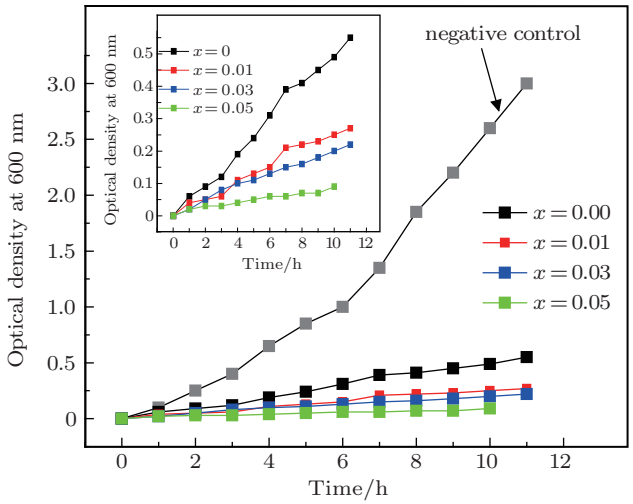


Fig. 7. (color online) Cu concentration dependent antibacterial activities of Cu-doped ZnO nanoparticles. Inset shows the sample plot of optical density in the range of 0–0.5 for better evaluation.

The disc diffusion method is adopted to examine the *in vitro* antibacterial activity of the synthesized nanoparticles against multi-drug resistant E. coli bacteria. Figure 8 illustrates the inhibition zone diameter (IZD) for pure and Cu-doped Zno nanoparticles. The antibacterial activity is shown by all the prepared samples. The bactericidal potency of nanoparticles increases with the Cu concentration, as can be seen in Fig. 8. Several mechanisms are responsible for the action of Cu-doped Zn nanoparticles against bacteria, which leads to the formation of IZD such as, decomposition of ZnO and the formation of reactive oxygen species, electrostatic interaction of nanomaterials with cell wall and photocatalytical light activation of ZnO nanomaterials.[38] The higher bactericidal potency for the $x = 0.05$ sample may be attributed to its smaller grain size compared to others, as it can be depicted from FESEM images. Due to the decrease in size, these nanoparticles are able to adhere with the cell wall of the organism, thus causing its destruction and causing death of the cells.[38] The Cu-doped ZnO nanoparticles are impartially stable for a period of 60 days at room temperature and they only lost 20% of antibacterial activity as tested against E. coli (data not shown here).

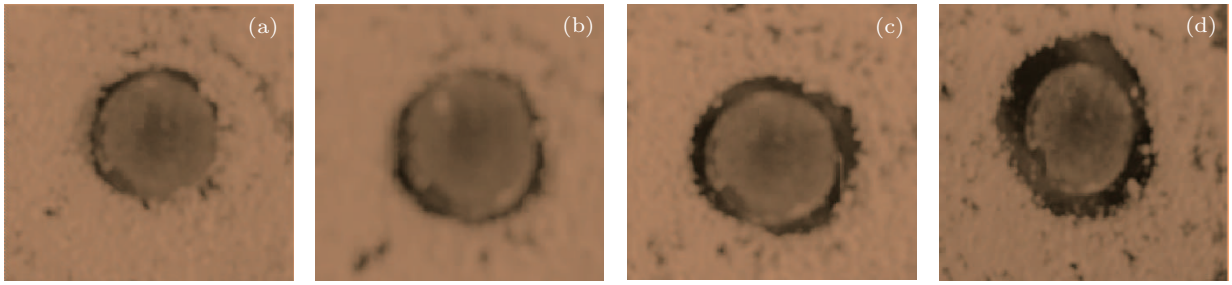


Fig. 8. (color online) Zone of inhibition formed by pure and Cu-doped ZnO nanoparticles against multi-drug resistant E. coli bacteria: (a) pure, (b) $x = 0.01$, (c) $x = 0.03$, and (d) $x = 0.05$.

4. Conclusions

Pure and Cu-doped ZnO nanoparticles are synthesized via a facile yet accurate sol-gel method. The considerable influences of Cu dopants on the spectroscopic characteristics and antibacterial activities are demonstrated. The incorporation of Cu in the ZnO matrix is found to alter the crystalline structures via defect mediated strain interactions and broadens the spectral width. This in turn modifies the lattice parameters and elastic constants of the single crystalline nanoparticles phase. The nanoparticles size estimation through different methods reveals consistent measures. The XRD measurement exhibits the wurtzite structure for $Zn_{1-x}Cu_xO$ without any pyrochlore phase at calcination temperatures of 600 °C. The XRD broadening is analyzed using the Scherrer plot. The crystallite size decreases from ~ 52 to ~ 30 nm with the increase of dopant (Cu) concentrations. The band gap energy calculated using PL and absorption spectra is blue shifted by increasing the Cu concentration. Furthermore, the bactericidal property is found to be concentration dependent and ZnO nanoparticles with 5% Cu dopants ($x = 0.05$) show the maximum inhibition against bacterial growth. Consequently, we can propose that Cu-doped ZnO nanoparticles can be used as an ingredient for the dermatological applications in lotions, creams, ointments, or other biomedical applications.

References

[1] Xue H, Chen Y, Xu X, Zhang G H, Zhang H and Ma S Y 2009 *Physica E: Low-dimensional Systems and Nanostructures* **41** 788
[2] Yuan Q, Hein and Misra R 2010 *Acta Biomaterialia* **6** 2732
[3] Law M, Greene L E, Johnson J C, Saykally R and Yang P 2005 *Nat. Mater.* **4** 455
[4] Ding H F, Yang H T, Liu L P, Xiao R, Song N N, Shen J, Zhang X Q, Cheng Z H and Zhao G P 2015 *Chin. Phys. B* **24** 027804
[5] Zhou H, Fang G, Yuan L, Wang C, Yang X, Huang H, Zhou C and Zhao X 2009 *Appl. Phys. Lett.* **94** 3503

[6] Ohira T, Yamamoto O, Iida Y and Nakagawa Z E 2008 *J. Mater. Sci.: Mater. Med.* **19** 1407
[7] Samavati A, Othaman Z, Ghoshal S and Mustafa M 2015 *Superlattices Microstruct.* **86** 134
[8] Tokumoto M S, Pulcinelli S H, Santilli C V and Briois V 2003 *J. Phys. Chem. B* **107** 568
[9] Baruwati B, Kumar D K and Manorama S V 2006 *Sens. Actuat. B: Chem.* **119** 676
[10] Cimitan S, Albonetti S, Forni L, Peri F and Lazzari D 2009 *J. Colloid Interf. Sci.* **329** 73
[11] Yadav R S, Mishra P and Pandey A C 2008 *Ultrason. Sonochem.* **15** 863
[12] Okada T, Agung B and Nakata Y 2004 *Appl. Phys. A* **79** 1417
[13] Ullah R and Dutta J 2008 *J. Hazardous Mater.* **156** 194
[14] Wang J, Huang G, Zhong X, Sun L, Zhou Y and Liu E 2006 *Appl. Phys. Lett.* **88** 252502
[15] Chen K J, Fang T H, Hung F Y, Ji L W, Chang S J, Young S J and Hsiao Y 2008 *Appl. Surf. Sci.* **254** 5791
[16] Nair M G, Nirmala M, Rekha K and Anukaliani A 2011 *Mater. Lett.* **65** 1797
[17] King S L, Gardeniers J and Boyd I W 1996 *Appl. Surf. Sci.* **96** 811
[18] Page K, Wilson M and Parkin I P 2009 *J. Mater. Chem.* **19** 3819
[19] Li J, Hong R, Li M, Li H, Zheng Y and Ding J 2009 *Progress in Organic Coatings* **64** 504
[20] Raghupathi K R, Koodali R T and Manna A C 2011 *Langmuir* **27** 4020
[21] Premanathan M, Karthikeyan K, Jeyasubramanian K and Manivannan G 2011 *Nanomedicine: Nanotechnology, Biology and Medicine* **7** 184
[22] Aruoja V, Dubourguier H C, Kasemets K and Kahru A 2009 *Sci. Total Environ.* **407** 1461
[23] Huang Z, Zheng X, Yan D, Yin G, Liao X, Kang Y, Yao Y, Huang D and Hao B 2008 *Langmuir* **24** 4140
[24] Sharma V, Shukla R K, Saxena N, Parmar D, Das M and Dhawan A 2009 *Toxicology Lett.* **185** 211
[25] Jones N, Ray B, Ranjit K T and Manna A C 2008 *FEMS Microbiology Lett.* **279** 71
[26] Zhang L, Jiang Y, Ding Y, Povey M and York D 2007 *J. Nanopart. Res.* **9** 479
[27] Cullity B 1978 *Elements of X-ray Diffraction*
[28] Gayen R, Das S, Dalui S, Bhar R and Pal A 2008 *J. Cryst. Growth* **310** 4073
[29] Sahar M and Budi A S 2006 *Solid State Sci. Technol.* **14115**
[30] Ozgur U, Alivov Y I, Liu C, Teke A, Reshchikov M, Dogan S, Avrutin V, Cho S and Morkocd H 2005 *J. Appl. Phys.* **98** 041301
[31] Dingle R 1969 *Phys. Rev. Lett.* **23** 579
[32] Garces N, Wang L, Bai L, Giles N, Halliburton L and Cantwell G 2002 *Appl. Phys. Lett.* **81** 622
[33] Ozgur U, Alivov Y I, Liu C, Teke A, Reshchikov M, Dogan S, Avrutin V, Cho S J and Morkoc H 2005 *J. Appl. Phys.* **98** 041301
[34] West C, Robbins D, Dean P and Hayes W 1983 *Physica B* **116** 492
[35] Soundarrajan P, Sankarasubramanian K, Sampath M, Logu T, Sethuraman K and Ramamurthi K 2015 *Physica E: Low-dimensional Systems and Nanostructures* **71** 56
[36] Grundmann M 2010 *Heidelberg*
[37] Bedir M, Öztas M, Yazici A N and Kafadar E V 2006 *Chin. Phys. Lett.* **23** 939
[38] Schwartz V B, Thétiot F, Ritz S, Pütz S, Choritz L, Lappas A, Förch R, Landfester K and Jonas U 2012 *Adv. Funct. Mater.* **22** 2376